P2.21 THE IMPACT OF CLOUD PROCESSING BY TRADE-WIND CUMULUS ON THE LIGHT SCATTERING EFFICIENCY OF AEROSOL PARTICLES

Justin R. Peter, Alan M. Blyth, J ørgen B. Jensen and Donald C. Thornton *

1. Introduction

Absorption and scattering of light by anthropogenic tropospheric aerosol particles (AP), is recognized as a major perturbation to the global radiation budget (Charlson et al., 1992; IPCC, 2001). The majority of anthropogenic AP is present in the form of sulfate ($\approx 75\%$ in the northern hemisphere (Koch et al., 1999)), formed by oxidation of gas-phase SO_2. Although oxidation of SO_2 can occur in both the gas and aqueous phases, the major pathway for the production of sulfate is aqueous-phase oxidation occurring within cloud droplets (Hegg, 1985; Langner et al., 1992; Laj et al., 1997). The oxidation of SO_2 to sulfate and the subsequent addition of mass to AP has been shown to result in their increased light scattering efficiency (Yuskiewicz et al., 1999) and hypothesised to have a concomitant cooling effect on climate (Lelieveld and Heintzenberg, 1992) comparable to the warming induced by greenhouse gases (IPCC, 2001). Additionally, the enhancement of aerosol mass may increase the activity of AP making them more effective cloud condensation nuclei (CCN) (Hegg et al., 1996) which will modify the microphysics of subsequent clouds that form on the cloud-processed aerosol from those clouds that form on non-cloud-processed AP (Khain et al., 1999; Hatzianastassiou et al., 1998).

In this paper we use conserved thermodynamic tracers, wet equivalent potential temperature and total water mixing ratio (θ_q and Q respectively) are used to characterize sub-saturated air parcels in a cloudy trade-wind cumulus layer. A mixing diagram of $\{\theta_q$,$Q\}$ samples close to a cloud shows that sub-saturated air, sampled at a constant altitude in the cloud layer upwind and downwind of a cloud band, is composed of air parcels that have originated from two levels; near cloud base and a level in the free troposphere. The only manner in which air from the sub-cloud layer can make its way into the free troposphere is via convection and, therefore, contains cloud-processed air. The largest values of θ_q identify air that has most recently been detrained from cloud and experienced less mixing with environmental air than air parcels with lower θ_q. As such, parcels with larger θ_q are more indicative of the effect of cloud processing on the aerosol particle and SO_2 concentration than parcels with a smaller θ_q. We stratify the aerosol size distribution, condensation nuclei concentrations, sulfur dioxide concentration and the aerosol extinction coefficient and mass extinction efficiency with θ_q. This enables physical interpretations about cloud processing of aerosol particles and SO_2 to be inferred. Although there is evidence of mass addition of sulfate to aerosol particles and an observable modification of the aerosol size distribution, we find no modification of the aerosol extinction coefficient nor the aerosol mass extinction efficiency.

*Corresponding author address: Justin R. Peter, Institute for Atmospheric Science, School of Earth and Environment, University of Leeds, Leeds, UK; e-mail: jpeter@env.leeds.ac.uk

2. Methodology

2.1 *Operational area and instrumentation*

The data reported here were obtained during the Rain In Cumulus over the Ocean (RICO) field campaign conducted off the Caribbean islands of Barbuda and Antigua during December 2004 and January 2005. RICO was designed to characterize trade-wind cumulus on all scales, from the microphysical to the mesoscale, with a particular focus on the initiation of precipitation via the warm rain mechanism (Rauber et al., 2004). The experimental location was in the area covered by the latitude range 17–19 $^\circ$S and longitude 70–76 $^\circ$E. At this location and time of year, trade-wind cumulus are ubiquitous, as is the prevailing trade-wind which is an easterly. Additionally, due to the marine location and prevailing wind the AP are expected to be primarily of marine origin since the nearest continental influence is north Africa over 4700 km distant (Savoie et al., 1989). The trade-wind cumulus layer at this time of year is characterized by shallow convection, the cloud layer extending a maximum of 4 km to the trade-wind inversion.

The measurement platform used was the NCAR-C130 aircraft, instrumented to measure several cloud, aerosol and meteorological parameters. Aerosol particle size distributions were measured with a PCASP, condensation nuclei (CN) and ultrafine condensation nuclei (UCN) were measured with a TSI Model 3760/3025 respectively. The aerosol light scattering extinction coefficient (b_{sp}) was measured with an integrating nephelometer (TSI Model 3563). Cloud liquid water content (LWC) was measured using a 260X emulation of a PMS 2D-C probe. Clear air temperature was measured with a Rosemount platinum resistance element. In-cloud temperature was calculated from humidity measurements made with a Lyman-α hygrometer and then assuming saturation. A summary of these instruments, the ones pertinent to the present analysis, is presented in Table 1.

We also examine a derived variable, the aerosol mass scattering efficiency α, which is the contribution of the aerosol scattering extinction coefficient (b_{sp} measured by the nephelometer) per unit aerosol mass. The equation relating b_{sp} and α is, b_{sp}=$\int_0^{r_p} \alpha n_m(r_p) dr_p$ where r_p and n_m are the AP radius and AP mass distribution function respectively (Seinfeld and Pandis, 1998; Yuskiewicz et al., 1999). The mass scattering efficiency was calcu-

lated assuming an AP density of 1.8×10^3 g kg^{-1}, representative of AP consisting mainly of sea salt and sulfate and, therefore, of a marine origin. We introduce the aerosol mass scattering efficiency as it is strongly dependent on particle size and, consequently, related to perceptible visibility via the Koschmeider equation (e.g. Seinfeld and Pandis, 1998, pg. 1128) and to aerosol optical and direct radiative forcing (Lelieveld and Heintzenberg, 1992). Due to the dependence of the aerosol mass scattering efficiency on particle size, α provides a more useful indication of the effect of mass addition to the AP size distribution on the aerosol optical properties than b_{sp}.

The results presented here are from a portion (1709:30–1725:00 UT) of a flight flown on the 19 January 2005, or Research Flight 17 (RF17). During this time the C-130 flew a constant altitude leg (at height $z\sim$1920 m asl) from SE to NW through a cloud band which was oriented in an E-W plane. Cloud base (top) was at an altitude of $\sim$550–600 m ($\sim$ 2500 m). In-cloud vertical velocities ranged from 1–4 m s^{-1}, which resulted in activation of aerosol with radii smaller than the efficient light scattering range ($\sim$ 0.1–0.3 μm), which is pertinent because mass added to AP smaller than this range may cause them to grow into the efficient light scattering regime.

3. Results and Discussion

3.1 *Qualitative evidence of cloud processing of AP and SO_2*

In Figure 1, time series obtained during RF17 of 1 Hz data are shown. The left hand side of the figure corresponds to air that was sampled downwind of the cloud band and the right hand side to that of air that was sampled upwind of the cloud band. The main cloud band was encountered at 1719:30 UT as evidenced by the trace of liquid water content (LWC) shown in Figure 1(a). Clouds of substantially lower liquid water content were also encountered downwind of the main band. The rest of the panels in Figure 1 provide some qualitative information about cloud processing of the AP size distribution.

Figure 1(b) shows that θ_q is about 5–6 K greater on the downwind side of the cloud band than on the upwind, which is due to convection transporting moisture and heat from the sub-cloud layer to the free troposphere. Convection will also transport AP and gas species from the sub-cloud layer to the free troposphere during which time the AP and gas will pass through cloud and undergo physical and chemical modification. Accordingly we expect that evidence of cloud processing of AP and gas species will exhibit itself as differences in measurements on the upwind and downwind sides of the cloud band.

The timeseries of AP concentration measured by the PCASP (Figure 1(c)) shows that aerosol concentrations were low at around 5 cm^{-3} but does not indicate any significant difference between concentrations on the upwind and downwind sides of the cloud band. Figure 1(c) shows that there is a substantial reduction of CN from $\sim$700 cm^{-3} upwind of the cloud band to $\sim$400 cm^{-3} downwind. The reduction is probably attributable to Brownian diffusion of the CN to cloud droplets. There is also a decrease in SO_2 concentration on the downwind side of the cloud band presumably due to the aqueous phase conversion of SO_2 to sulfate inside cloud droplets. Finally, despite Figure 1 providing some qualitative evidence that there has been scavenging of CN and uptake of SO_2 within the cloud, Figure 1(f) reveals that there has been no modification of the aerosol optical properties from the upwind to the downwind side of the cloud band, however, a more quantitative investigation is required.

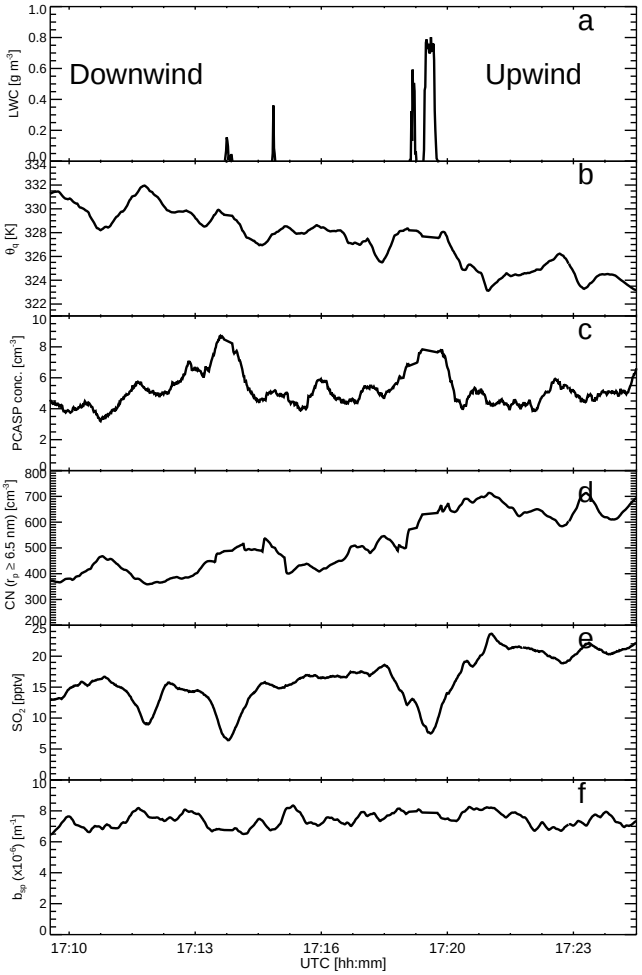

FIG. 1: Timeseries of (a) liquid water content, (b) wet equivalent potential temperature, (c) aerosol concentration measured by the PCASP, (d) condensation nuclei with particle radius $r_p \geq$ 6.0 nm measured with a TSI-3760, (e) SO_2 concentration measured with an APIMS, and (f) aerosol scattering coefficient measured with a nephelometer. See Table 1 for instrument details. Qualitative evidence of uptake of CN and SO_2 within the cloud band is evidenced by the decrease in both of these quantities from the upwind to the downwind side of the cloud band.

3.2 *Quantitative evidence of cloud processing of AP and SO_2*

3.2.1 SOURCE OF SUB-SATURATED CLOUD-LAYER AIR

Figure 2 shows a mixing diagram of wet equivalent potential temperature (θ_q) and total water mixing ratio (Q). Wet equivalent potential temperature (total water mixing ratio) is conserved if no diabatic (irreversible) processes occur. In the current situation both of these criteria are met as the heating (cooling) adjustment due to gain (loss) of heat from longwave radiation acts on a timescale much greater than the observation period, and the cloud system observed was not precipitating. Since θ_q and Q are conserved, linear mixing between air parcels will present itself as a straight line of $\{\theta_q,Q\}$ samples on the mixing diagram. The technique of using conserved quantities to form the coordinate axes has been applied to the study of mixing processes in cumulus clouds (Paluch, 1979; Blyth et al., 1988) and to conceptual models of convection (Raymond and Blyth, 1986).

There are four sets of data plotted in Figure 2: the thick curve is observations of 1 Hz $\{\theta_q,Q\}$ samples from a clear-air sounding upwind of the cloud band; the large circle is the thermodynamic state of cloud base; closed circles are 1 Hz samples of cloudy air; open circles are 1 Hz samples of clear air. The cloud base value was obtained from sub-cloud measurements of temperature and water vapor mixing ratio, which were then iterated to the lifting condensation level. Cloudy air has been defined as samples with a LWC greater than 0.4 g kg^{-1} and clear air with an LWC less than 1×10^{-3} g kg^{-1}.

Two pieces of information can be obtained from mixing diagrams. First, the source of each of the cloudy and clear air samples. The line of best fit connecting the the cloudy and clear air samples passes through the cloud base sample and a level on the sounding, which means that each of the cloudy and clear air samples contain air parcels that originated from near cloud base and the altitude at which the line of best fit (LOBF) intersects the sounding, known as the Primary Source of Entrained Air (PSEA) (Jensen et al., 1985). Second, because θ_q and Q are conserved quantities, the relative distance of a sample bewteen the cloud base sample and the PSEA will give the unit mass of the clear or cloudy air sample that has originated from cloud base (known as the F-fraction) (Jensen et al., 1985; Peter et al., 2005).

Examination of Figure 2 reveals that the PSEA for the clear air samples (PSEA$_{clear}$), using all clear air samples for its determination, is $\sim$2400 m. The PSEA, however, is not a discrete location but should be considered the mid-point of a region on the sounding. By constructing a LOBF between the cloud base sample and the extreme values of θ_q for the clear air samples we can determine the extrema of PSEA$_{clear}$. This method gives a range for PSEA$_{clear}$ of 2000–2700 m. The fraction of air originating from near cloud base F$_{clear}$, ranges from 0–0.5 for the clear air samples. Knowledge of the vertical profile of aerosol and SO_2 concentrations, the PSEA$_{clear}$ and F$_{clear}$ allows us to estimate the AP and SO_2 concentrations that we expect based on a mixing analysis. For clear air samples that have F$_{clear}$=0, the concentration of AP and SO_2 should be that measured at the PSEA$_{clear}$, which from Figure 3 is $\sim$3 cm^{-3} and $\sim$15 pptv respectively. For clear air samples that have F$_{clear}$=0.5, then we expect 50% of the contribution of AP and SO_2 to come from the sub-cloud concentration and the remaining 50% from the concentration at the PSEA$_{clear}$. The sub-cloud concentration of aerosol and SO_2 is 25 cm^{-3} and 15 pptv respectively, giving an expected concentration of 14 cm^{-3} for AP and 15 pptv for SO_2 (for air parcels with F$_{clear}$=0.5).

For the current discussion, the most important information revealed by Figure 2 is, during the constant altitude flight leg of RF17 there are clear air samples that

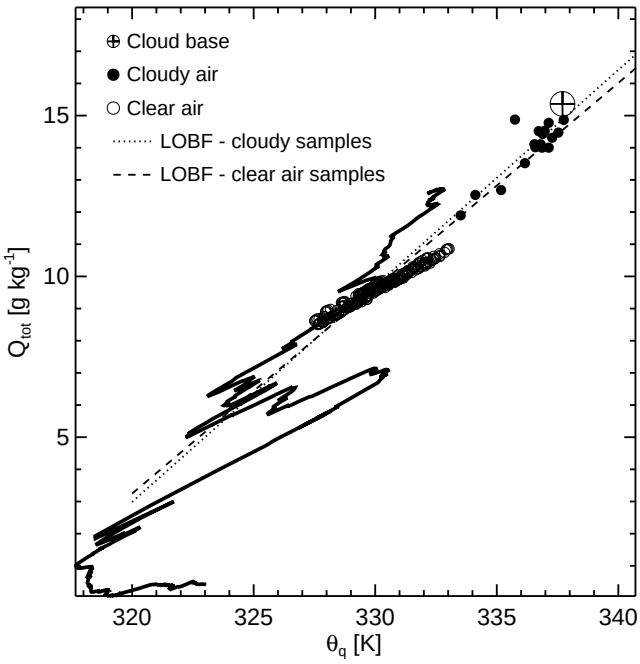

FIG. 2: Mixing diagram of conserved variables, total water content (Q) and wet equivalent potential temperature (θ_q). Cloudy (clear-air) 1 Hz samples are shown as filled (open) circles. The distance of a sample from the cloud base sample indicates the proportionate amount of cloud base and environmental air that it contains, known as the F-fraction. Samples with a larger value of θ_q therefore contain more air that has originated from cloud base than samples with a smaller value of θ_q. A corollary is that samples with a larger value of θ_q exhibit the greatest "signature" of cloud processing. This signature of cloud processing of the AP size distribution is exemplified in the emergence of a peak as θ_q increase at a particle radius of r$_p\approx$0.9μm in the AP size distribution shown in Figure 4.

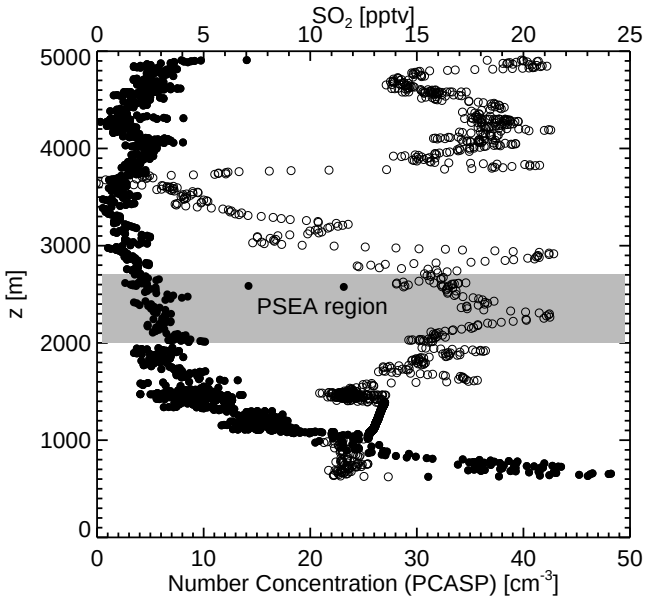

FIG. 3: Vertical profiles of AP number concentration measured by the PCASP (solid circles) and SO_2 concentration (open circles). The sounding corresponds exactly to the sounding curve of Figure 2. The PSEA of clear air samples determined from mixing analysis is indicated by the shaded region.

have a fraction of air that has originated from below cloud base. The only manner in which sub-cloud air can make its way into the cloud layer is via convection and, necessarily, transport through cloud. There are also clear air samples that lie on the same curve as the sounding samples and therefore have not necessarily been cloud processed but are more representative of the background air at the flight altitude. It is also evident from Figure 2 that samples with a larger θ_q have a larger fraction of air that has originated from sub-cloud than those samples with a smaller θ_q. Correspondingly, we expect samples with a larger θ_q to be those that have most recently been detrained from cloud and experienced the least amount of mixing with non-cloud-processed environmental air.

3.3 *Effect of cloud processing on AP and SO_2*

Figure 4 shows AP size distributions stratified with θ_q, in 1 K intervals, for all 1 Hz clear-air samples during the flight leg of RF17. We have used the criteria that each of the Gerber, FSSP and 2D-C probes measure a LWC of less than 1×10^{-3} g kg^{-1} to define clear air, such that the AP size distributions correspond exactly to the clear air samples of Figure 2. The color scale at the top of the figure gives the value of θ_q at which each of the AP size distributions were sampled. The inset shows the frequency distribution of the number of samples in each 1 K θ_q interval. The black line shows the time-averaged AP size distribution over all 1 Hz clear-air samples. There is an apparent positive stratification of the AP size distribution with θ_q. Especially noticeable is the emergence of an extra mode at around $r_p \approx 0.9$ μm as θ_q increases, which (as we will show) we attribute to the addition of mass to the AP size distribution due to aqueous phase processing of SO_2.

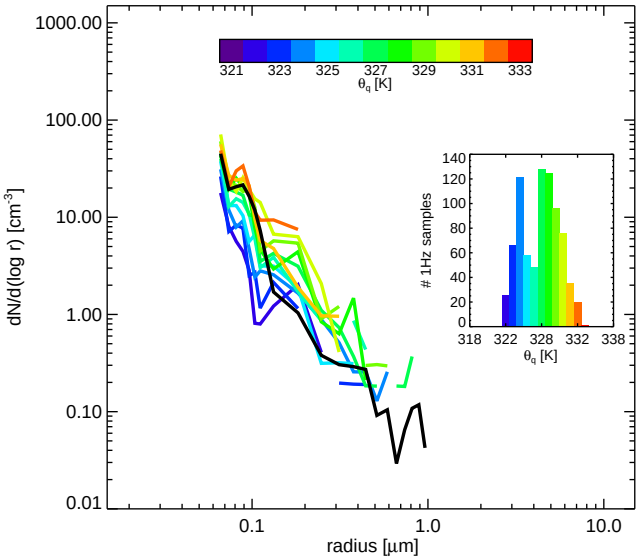

FIG. 4: Clear-air AP size distributions stratified with wet equivalent potential temperature (θ_q) in 1 K increments. The color bar indicates the value of θ_q. The inset is a histogram of the number of samples in each θ_q interval. The black line is the time-averaged aerosol size distribution.

Clear air samples with larger θ_q are those that contain the largest fraction of sub-cloud air (where θ_q is largest) and have therefore been recently detrained from cloud and had the least amount of mixing with non-cloud-processed air. Samples with a smaller value of θ_q are those that, even though they may have experienced some time in cloud, have experienced proportionately more mixing with non-cloud-processed air than the samples with larger θ_q. There is thus a series of θ_q AP size distributions ranging from a minimum θ_q of 320 K, representative of non-cloud-processed background air, to a maximum θ_q of 332 K, representative of recently cloud detrained air parcels which, therefore, exhibit the greatest "signature" of cloud processing.

The emergence of a peak in the AP size distribution at a radius of $r_p \approx 0.9$ μm, is indicative of mass being added to the AP size distribution. Figure 5 reveals more details of the processes controlling the addition of mass to the AP size distribution. It shows the averages of quantities (UCN, CN, PCASP AP and SO_2 concentrations and nephelometer extinction coefficient) averaged in 1 K θ_q bins. The CN and SO_2 concentrations have a negative correlation with θ_q. The SO_2 concentration (Figure 5(e) decreases from $\sim$22 pptv to $\sim$8 pptv. From the previous mixing argument, we expected that the SO_2 concentra-

tion should be about 15 pptv. It is seen that many of the values do in fact correspond to this, however, there are concentrations above and below this. Values greater than 15 are readily explainable, as the SO_2 concentration in the PSEA reaches peak values of 25 pptv. However, the mixing analysis cannot account for SO_2 concentrations below 15 pptv. Therefore, some of the negative correlation of θ_q and SO_2 concentration exhibited in Figure 5(f) can be explained by mixing, however, SO_2 concentrations below 15 pptv for larger values of θ_q must be due to loss within cloud. Similar arguments hold for the negative correlation of UCN and CN concentrations with θ_q.

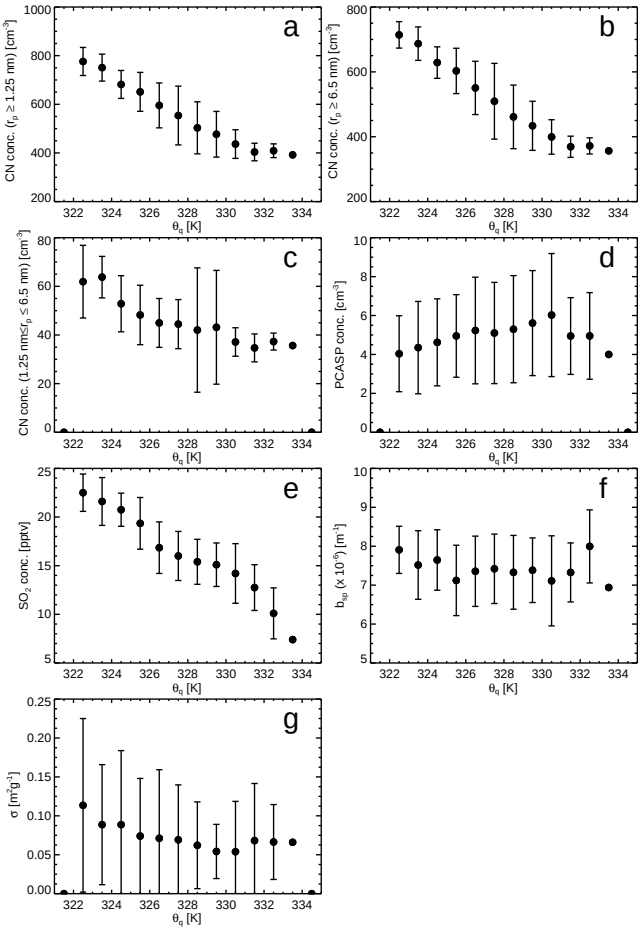

FIG. 5: Average values of UCN, CN, PCASP and SO_2 concentrations, aerosol extinction coefficient and aerosol mass scattering efficiency. A one standard deviation range of variability is shown for each quantity in a 1 K θ_q interval.

Recalling that air parcels with a larger value of θ_q are parcels that exhibit signatures of cloud processing, it seems that the decrease of CN and SO_2 concentrations is due to in-cloud scavenging. Particles measured by the TSI CN counters have small radii and therefore large diffusion coefficients, that results in them being scavenged by Brownian diffusion to cloud droplets while SO_2 undergoes scavenging and aqueous-phase oxidation within cloud droplets. The peak that appears in the AP size distribution at $r_p \approx 0.9$ μm can therefore be attributed to the addition of mass via the aqueous-phase oxidation of sulfur dioxide. This is a well established phenomena (Hoppel et al., 1986), though the method of stratifying AP size distributions, particle concentrations and other quantities via θ_q enables the effect of sulfate production to be more readily observed than comparing sub-cloud and detrained AP size distributions.

The process under investigation here, however, is the effect of the addition of mass to the AP size distribution on the AP light scattering efficiency. Despite the conversion of SO_2 to sulfate and the observable modification of the AP size distribution, Figure 5(f) indicates that there is little, if no, effect on the aerosol light scattering properties. A possible explanation for this is that the ambient SO_2 concentration is too low to modify the optical properties of the AP. Another possibility is that the emergence of the mode may be due, in part, to collision-coalescence of cloud droplets within cloud. Collision-coalescence of cloud droplets will modify the detrained AP size distribution in a manner similar to aqueous-phase conversion of SO_2 to sulfate; by increasing the mean size of the AP detrained from the cloud relative to the input AP (Feingold et al., 1996). Furthermore, Feingold et al. (1996) found that the increase in AP mean mass via cloud droplet collision-coalescence is comparable to that induced by aqueous-phase production of sulfate for clouds with a LWC $\geq$ 0.5 g m^{-3}, which is of the same order of magnitude as the cloud band examined (see Figure 1(a)). Although we can not discount the contribution of cloud droplet collision-coalescence to the appearnce of the mode in Figure 4, the preceding mixing argument coupled with the results presented in Figure 5 clearly highlights that aqueous-phase processing of SO_2 is contributing to the appearance of the mode. Regardless of which processes are contributing to the mode in the AP size distribution, Figure 5(f) demonstrates that, in this case, neither process is modifying the aerosol mass scattering efficiency.

Finally, we mention that though the results presented here are conclusive, we have only examined one cloud band. This was due to SO_2 data only being available for RF17. When the complete RICO SO_2 data set becomes available a similar analysis to that presented will be enabled. Furthermore, the results presented here were from a flight that was specifically designed to study one cloud in detail, however, the method of stratifying AP size distributions detailed here can be applied to any flight pattern. In particular, statistical flights were flown during RICO where the aircraft penetrated many clouds at many altitudes. The current analysis applied to such flight patterns will enable conclusions about the statistical nature of cloud processing of AP and SO_2 by an ensemble of trade-wind cumulus.

REFERENCES

Blyth, A., W. Cooper, and J. Jensen, 1988: A study of the source of entrained air in Montana cumuli. *J. Atmos. Sci.*, **45**, 3944–3964.

Charlson, R., S. Schwartz, J. Hales, R. Cess, J. Coakley, J. Hansen, and D. Hofmann, 1992: Climate forcing by anthropogenic aerosols. *Science*, **255**, 423–430.

Feingold, G., S. Kreidenweis, B. Stevens, and W. Cotton, 1996: Numerical simulations of stratocumulus processing of cloud condensation nuclei through collision-coalescence. *J. Geophys. Res.*, **101**(D16), 21,391–21,402.

Hatzianastassiou, N., W. Wobrock, and A. Flossmann, 1998: The effect of cloud-processing of aerosol particles on clouds and radiation. *Tellus*, **50B**, 478–490.

Hegg, D., 1985: The importance of liquid-phase oxidation of SO_2 in the atmosphere. *J. Geophys. Res.*, **90**, 3773–3779.

Hegg, D., R. Majeed, P. Yuen, M. Baker, and T. Larson, 1996: The impacts of SO_2 oxidation in cloud drops and in haze particles on aerosol light scattering and CCN activity. *Geophys. Res. Lett.*, **23**, 2613–2616.

Hoppel, W., G. Frick, and R. Larson, 1986: Effect of nonprecipitating clouds on the aerosol size distribution in the marine boundary layer. *Geophys. Res. Letters*, **13**, 125–128.

IPCC, 2001: The Scientific Basis. Contribution of Working Group 1 to the Third Assessment Report of the Intergovernmental Panel on Climate Change. In *Climate Change 2001*, Houghton, J., Ding, Y., Griggs, D., Noguer, M., van der Linden, P., Dai, X., Maskell, K., and Johnson, C., editors. Cambridge University Press, Cambridge, United Kingdom and New York, NY, USA, 881.

Jensen, J., P. Austin, M. Baker, and A. Blyth, 1985: Turbulent mixing, spectral evolution and dynamics in a warm cumulus cloud. *J. Atmos. Sci.*, **42**, 173–192.

Khain, A., A. Pokrovsky, and I. Sednev, 1999: Some effects of cloud-aerosol interaction on cloud microphysics structure and precipitation formation: numerical experiments with a spectral microphysics cloud ensemble model. *Atmos. Res.*, **52**(3), 195–220.

Koch, D., D. Jacob, I. Tegen, D. Rind, and M. Chin, 1999: Tropospheric sulfur simulation and sulfate direct radiative forcing in the Goddard Institute for Space Studies general circulation model. *J. Geophys. Res.*, **104**, 23,799–23,823.

Laj, P., S. Fuzzi, M. Facchini, G. Orsi, A. Berner, C. Kruisz, W. Wobrock, A. Hallberg, K. Bower, M. Gallagher, K. Beswick, R. Colville, T. Choularton, P. Nason, and B. Jones, 1997: Experimental evidence for in-cloud production of aerosol sulfate. *Atmospheric Environment*, **31**(16), 2503–2514.

Langner, J., H. Rodhe, P. Crutzen, and P. Zimmermann, 1992: Anthropogenic influence on the distribution of tropospheric sulphate aerosol. *Nature*, **359**, 712–716.

Lelieveld, J. and J. Heintzenberg, 1992: Sulfate cooling effect on climate through in-cloud oxidation of anthropogenic SO_2. *Science*, **258**, 117–120.

Paluch, I., 1979: The entrainment mechanism in Colorado cumuli. *J. Atmos. Sci.*, **36**, 2462–2478.

Peter, J., S. Siems, J. Jensen, J. Gras, Y. Ishizaka, and J. Hacker, 2005: Prediction and observation of cloud processing of the aerosol size distribution by a band of cumulus. *Accepted for publication in Q. J. R. Meteorol. Soc.*

Rauber, R., H. Ochs, C. Knight, and B. Stevens, 2004: *RICO Operations Plan*, 134.

Raymond, D. and A. Blyth, 1986: A stochastic mixing model for nonprecipitating cumulus clouds. *J. Atmos. Sci.*, **43**(22), 2708–2718.

Savoie, D. L., J. M. Prospero, and E. S. Saltzman, 1989: Non-sea-salt sulfate and nitrate in trade wind aerosols at barbados: Evidence for long-range transport. *J. Geophys. Res.*, **94**, 5069–5080.

Seinfeld, J. and S. Pandis, 1998: *Atmospheric chemistry and physics; from air pollution to climate change*. John Wiley and Sons, Inc., New York.

Yuskiewicz, B., F. Stratmann, W. Birmili, A. Wiedensohler, E. Swietlicki, O. Berg, and J. Zhou, 1999: The effects of in-cloud mass production on atmospheric light scatter. *Atmos. Res*, **50**, 265–288.